Applied Catalysis A, General 613 (2021) 118021

Contents lists available at ScienceDirect

Applied Catalysis A, General

journal homepage: www.elsevier.com/locate/apcata

Radical α–alkylation of ketones with unactivated alkenes under catalytic and sustainable industrial conditions

Sergio Sanz-Navarro [a,1], Francisco Garnes-Portolés [a,1], Carlos López-Cruz [b], Estela Espinós-Ferri [b], Avelino Corma [a], Antonio Leyva-Pérez [a,*]

[a] Instituto de Tecnología Química (UPV–CSIC), Universidad Politècnica de València, Consejo Superior de Investigaciones Científicas, Avda. de los Naranjos s/n, 46022, Valencia, Spain

[b] International Flavours & Fragrances Inc., Avda Felipe Klein 2, 12580, Benicarló, Castellón, Spain

ARTICLE INFO

Keywords:
Catalysis
Aerobic sustainable industrial reactions
α–alkylation
Manganese
Zeolites

ABSTRACT

The industrially–viable aerobic α–alkylation of cyclic and acyclic ketones with allyl and alkyl alkenes in the presence of catalytic amounts of Mn^{2+}, under homo– and heterogeneous conditions, is achieved here. The substitution of organic peroxides by Mn^{2+} either as a simple soluble salt or supported in zeolites, in air, generates in–situ peracid radicals and circumvents the aggressiveness of current industrial protocols, to pave the way for the design of sustainable aerobic catalytic systems. Combined reactivity and mechanistic studies show that large cyclic ketones stabilize a radical in the α–position due to a higher polarizability, steric hindrance and no proximity effects. As a proof of concept, the gram–scale synthesis of the industrial fragrance exaltolide is carried out with the Mn^{2+} catalysts in air, which clearly improves any other previously reported method not only in safety and environmental terms but also in number of synthetic steps and overall yield.

1. Introduction

The α–alkylation of ketones by coupling of deprotonated ketones with nucleofuge–containing molecules, under strong basic conditions, is a fundamental reaction in organic synthesis, in both industry and academia [1]. However, this low atom–efficient approach requires additional reagents to avoid competitive *O*–alkylations, which makes them industrially unviable in many cases. Modern procedures based on a combination of metal catalysts with spatially–directing amine additives have allowed the use of alkenes as coupling partners, which avoid any waste generation, however, the expensive catalysts/reagents employed in these protocols make them difficult to implement at industrial scale [2].

Fig. 1 shows that a full atom–economy alternative to enolates and/or complex metal systems consists in the use of α–radical ketones, which will naturally couple with simple alkenes [3]. However, the generation of the radical ketone generally triggers a plethora of other radical intra– and inter–molecular reactions, such as dimerization, transannular reaction, radical walking and different rearrangements, among others, and only the combination of different metal salts has somewhat circumvented these by–reactions so far [4]. Here, we envisioned that the higher polarizability, lack of proximity effects [5] and more severe steric hindrance compared with shorter ketones [6] of large cyclic ketones ($\geq C_{12}$) and, in general, long alkyl ketones, may allow to stabilize a radical in the α position, in such a way that a simple metal catalyst could rapidly perform the coupling with unactivated alkenes. If so, intra– and intermolecular reactions will be significantly avoided, and considering that α–alkylated (large cyclic) ketones are key intermediates in the fine chemical industry, [7] this particular reactivity deserves attention.

We show here that large cyclic and alkyl ketones couple with unactivated alkenes in the presence of catalytic amounts (1–2 mol%) of isolated Mn^{2+} atoms in zeolites and the non–toxic and inexpensive Mn $(OAc)_2{\cdot}4H_2O$ salt in the homogeneous phase, [8a–e] under air at 130 °C, and using the biomass–derived compound hexanoic acid as a solvent [8f].Notice that Mn^{2+} is used here in catalytic amounts, which differs significantly of the well–known Mn^{3+}–mediated reactions, which to become catalytic requires high amounts (up to 50 mol%) of mixed Mn compounds [8g]. The reaction protocol presented here is fully sustainable, industrially implementable, and does not show any toxicity and flammability limitations, which significantly improve the current

* Corresponding author.
E-mail address: anleyva@itq.upv.es (A. Leyva-Pérez).
[1] These authors contributed equally to the work.

https://doi.org/10.1016/j.apcata.2021.118021
Received 2 November 2020; Received in revised form 31 December 2020; Accepted 25 January 2021
Available online 29 January 2021

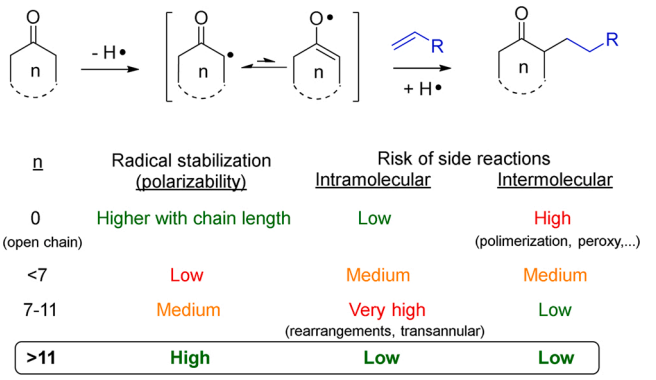

Fig. 1. Feasibility of the full–atom economic radical α–alkylation of ketones with alkenes. Color code: Positive (green), neutral (orange), negative (red).

industrial process based on sub–stoichiometric amounts of the radical initiator di*tert*–butyl peroxide (DTBP). A comparative mechanism study will show that a four–step, one–electron transfer chain occurs during the catalytic process, from Mn^{2+} to molecular oxygen then to the organic acid and finally to the ketone, thus circumventing the much more energetic direct organic peroxide abstraction. These findings have led to a new synthesis of the multi–ton industrial fragrance exaltolide, based on the aerobic radical procedure.

2. Materials and Methods

2.1. General

Reagents and solvents were obtained from commercial sources (Aldrich) and were used without further purification otherwise indicated. All the products obtained were characterised by GC–MS, ^{1}H, ^{13}C-NMR, and DEPT. When available, the characterisation given in the literature was used for comparison. Gas chromatographic analyses were performed in an instrument equipped with a 25 m capillary column of 5% phenylmethylsilicone. GC/MS analyses were performed on a spectrometer equipped with the same column as the GC and operated under the same conditions. ^{1}H, ^{13}C, and DEPT were recorded in a 300 MHz instrument using the appropriate solvent containing TMS as an internal standard. X-ray powder diffraction measurements were carried out, before and after catalysis, in a powder diffractometer using Cu Kα radiation (λ =1.54056 Å). Fourier-transformed infrared spectra (FT-IR) of the solids were recorded on a Jasco instrument by direct pressure on the measurement window. High-resolution field emission scanning electron microscopy (HR-FESEM) was performed in a Zeiss Ultra 55 model, by impregnating dispersions of the zeolites on the FESEM sampleholder and leaving to evaporate the solvent. X-ray photoelectron spectroscopy (XPS) measurements were performed by sticking, without sieving, the zeolite onto a molybdenum plate with scotch type film, followed by air drying. Measurements were performed using non–monochromatic Mg KR (1253.6 eV) X–ray source working at 50 W.

2.2. Synthesis of catalysts

2.2.1. Synthesis of the ditert-butylperester

Di*tert*butylperoxide DTBP (900 mg, 10 mmol) and pyridine (800 mg, 10 mmol) are dissolved in pentane (10 mL) in a 50 mL round-bottomed flask equipped with a stirring magnetic bar, and the solution cooled at -10 °C. Then, a solution of oxalyl chloride (530 mg, 4 mmol) in pentane (5 mL) is added dropwise. The pyridinium chloride was filtered and washed with pentane. The combined filtrate was cooled in a dry ice-acetone mixture and allowed to stand about 15 min to precipitate the perester as fine white crystals. The perester was collected quickly on a sintered glass filter, dissolved in a minimal amount of pure pentane at room temperature and the solution dried with magnesium sulfate, to give 900 mg of pure solid compound according to ^{1}H NMR.

2.2.2. Synthesis of the ditert-butylperoxinitrite

Anhydrous $ZnCl_2$ (20 mmol) was added to a solution of sodium *trans*-hyponitrite hydrate ($Na_2N_2O_2{\cdot}xH_2O$, 1.9 g, 18 mmol) and *tert*-butyl-bromide (17 mL, 150 mmol) in Et_2O (10 mL) and stirred for 1.5 h at 25 °C. The inorganic salt was filtered off and the organic phase was washed with H_2O. The aqueous phase was extracted with Et_2O and the combined organic layers were washed with water, dried over anhydrous Na_2SO_4 and concentrated under reduced pressure at 25 °C (bath temperature) to afford a solid crude product. Recrystallization from pentane provided DTBHN as crystalline white long needles.

2.2.3. Impregnation of $Mn(OAc)_2$ in zeolites

To a beaker with 2 g of the corresponding zeolite, a solution of Mn $(OAc)_2$ (1.82 mmol, 315 mg, 5% wt of Mn) in 2 mL of H_2O (0.9 M) was added. This mixture, was mixed with a spatula until obtaining a homogeneous paste, this paste was heated at 100 °C in an oven for 24 h.

2.2.4. Exchange of $Mn(OAc)_2$ in zeolites

In a round bottom flask with 2 g of the corresponding zeolite, a 0.7 M solution of $Mn(OAc)_2$ in H_2O (5 mL) was added. This mixture was stirred for 16 h at 25 °C, then vacuum filtered and washed with water. Once washed, the solid was transferred to a beaker and heated at 60 °C for 16 h. The Mn loading of the solid was determined by inductively coupled plasma-atomic emission spectroscopy (ICP-AES) technique, after disaggregation of the solid in aqueous acid mixture.

2.3. Catalytic studies

2.3.1. General reaction procedure for the Mn^{2+}-catalyzed reaction

The corresponding amounts of $Mn(OAc)_2{\cdot}4H_2O$ (for heterogeneous catalysis, the appropriate amount of solid catalyst to have 2 mol% of Mn^{2+} in the reaction, typically 130 mg, was added) and CDDK **2** (2.16 g, 12 mmol) were placed in a 6 mL vial equipped with a magnetic stirrer. AcOH (1 mL) or hexanoic acid (1−2 mL), and allyl alcohol **1a** (88 μL, 1.2 mmol) or allyl acetate **1b** (128 μL, 1.2 mmol) were then added and the vial was sealed, connected to a manometer. Oxygen was introduced through a valve to reach 10 bar and liberated to purge the vial. This operation was repeated twice to finally leave 10 bar oxygen atmosphere (c.a. 3 mmol, in principle none of the reactants and products ketone, alcohol or ester and carboxylic acid have a dangerous explosion index under molecular oxygen). The vial was placed in an oil-bath at 80 or 110 °C and stirred for the required time. After that, the vial was cooled, remaining oxygen liberated, and the mixture was analyzed by GC after dilution in dichloromethane (previous filtration for solid catalysts).

2.3.2. Reaction procedure for best results in Table 1

$Mn(OAc)_2{\cdot}4H_2O$ (2.8 mg, 1 mol%) and CDDK **2** (430 mg, 2.4 mmol for 2:1, entry 15; 860 mg, 4.8 mmol for 4:1, entry 16) were placed in a 6 mL vial equipped with a magnetic stirrer. AcOH (0.5 mL) and allyl acetate **1b** (128 μL, 1.2 mmol) were then added and the vial was sealed, connected to a manometer. Oxygen was introduced through a valve to reach 10 bar and liberated to purge the vial. This operation was repeated twice to finally leave 10 bar oxygen atmosphere (c.a. 3 mmol, in principle none of the reactants and products ketone, alcohol or ester and carboxylic acid have a dangerous explosion index under molecular oxygen). The vial was placed in an oil-bath at 130 °C and stirred for 3.5 h. After that, the vial was cooled, remaining oxygen liberated, and the mixture was analyzed by GC after dilution in dichloromethane.

2.3.3. Catalyst leaching study

Two identical reactions were set up, as indicated in the general procedure with Mn^{2+}-heterogeneous catalysts. After 15 min of reaction, an aliquot (50 μL) of the two reactions was taken, and one of them was

Table 1
Catalytic results for the radical coupling of CDDK 2 with allyl derivatives 1a–d under air.

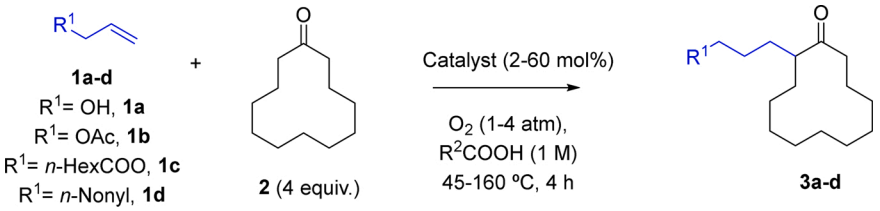

Entry	Catalyst (mol%)	Alkene	R^2	O_2 (atm)	T (ºC)	3 (%)
1[a]	(^{t}BuO)$_2$ (DTBP, 5)					11
2[a]	(^{t}BuO)$_2$ (15)				140	15
3[a]	H_2O_2 (15)	**1a**				<5
4[a]	(BnO)$_2$ (15)					9
5[a]	**(*t*BuO)$_2$ (15)**					**19**
6[a]	**(*t*BuO)$_2$ (30)**				**160**	**25**
7[a]	**(*t*BuO)$_2$ (30)**	**1b**				**14**
8[a]	**(*t*BuO)$_2$ (60)**					**21**
9[a]	(^{t}BuCOO)$_2$ (15)				45	7
10[a]	(^{t}BuON)$_2$ (15)				60	9
11	V_2O_5 (5)					<5
12	$FeCl_2$ (5)			Air		<5
13	$FeCl_3$ (5)		Me			<5
14	CuCl (5)					<5
15	$CuCl_2$ (5)	**1a**				<5
16	$CoCl_2$ (5)					<5
17	Co(OAc)$_2$ (5)					<5
18	Pd(OAc)$_2$ (5)				110	<5
19	ZnO (5)					<5
20	CeO_2 (5)					<5
21	Mn(OAc)$_2$ (5)					8
22	Mn(OAc)$_2$·4H_2O (5)					9
23		**1b**				13
24		**1a**				**15**
25		**1b**		**4**		**37**
26	**Mn(OAc)$_2$·4H_2O (2)**					**41**
27		**1c**				**52**
28				**4 + 20 N_2**		**55**
29		**1d**				**58**
30	MnO		***n*–Hex**			16
31	$MnCl_2$	**1c**		**4**		20
32	Mn_2O_3				**130**	27
33	MnO_2					32
34	$FeCl_3$ (5)					<5
35	Fe(acac)$_3$ (5)					<5
36	CuCl (5)	**1b**	Me	4		<5
37	Cu(OAc)$_2$ (5)					<5
38	Co(OAc)$_2$ (5)					<5

[a] Without AcOH solvent, increasing O_2 pressure has no effect on the reaction.

filtered in hot through a 20 μm nylon filter to remove all the solids. The resulting solution was reacted under exactly the same conditions and aliquots of both reactions were taken at 30, 60, 120 and 180 min. All aliquots were diluted with EtOAc (1 mL), filtered with a 20 μm nylon filter and analyzed by GC after adding *n*-dodecane (22 μL, 0.1 mmol) as an external standard.

2.3.4. Recovery and reuse of Mn^{2+}-NaBeta

The α-alkylation reaction of **2** with **1b** was performed using the general method and, after 4 h reaction time, the reaction was stopped and the zeolite separated from the solution using a centrifuge at 6000 rpm. After separation, the zeolite was cleaned with EtOAc (5 mL) and separated again in the centrifuge. The process was repeated twice. Then, the zeolite was left to dry overnight, weighed and used again in reaction, adjusting the mass of substrates and volume of hexanoic acid to keep the same final concentration.

2.4. Studies on the DTBP-mediated process

2.4.1. g-scale experimental procedure with DTBP radical initiator and isolation of the products

CDDK **2** (2.7 g, 15 mmol), allyl alcohol **1a** or allyl acetate **1b** (1.1 or 1.6 mL respectively, 1 equivalent) and peroxide DTBP (0.3 and 1.2 mL, 15 and 60 mol% respectively) are placed in a two-necked 25 mL round-bottomed flask equipped with a magnetic stir bar and a condenser, and heated in an oil bath at 140 °C or 160 °C, respectively, for 2.5 h. After that time the mixture is cooled, an aliquot is taken for GC analysis, and the crude is dissolved in CH_2Cl_2 (2 mL) and directly submitted to flash column chromatography on silica gel, eluting with a mixture of hexane and ethyl acetate. Rf (ketoalcohol, 30 % AcOEt) = 0.23. Rf (ketoester, 5% AcOEt) = 0.26. Yield of ketoalcohol: 240 mg (7%). Yield of ketoester: 1.0 g (23 %).

2.4.2. Experimental procedure for 4:1 ketone:alcohol ratio with DTBP peroxide catalyst

CDDK **2** (10.94 g, 60 mmol) was placed in a two-necked 25 mL round-bottomed flask equipped with a magnetic stir bar, a pressure-

compensated addition funnel and a condenser, and heated in an oil bath at 140 °C. A solution of *tert*-butyl peroxide DTBP (0.44 mL, 15 mol%) in allyl alcohol **1a** (1.1 mL, 15 mmol) was poured into the addition funnel and added dropwise during 6 h. After that time, the mixture was left to stir at 140 °C for additional 3 h and then the excess CDDK was distilled off (107 °C, 13 mmHg, 95 % recovering). Then, phosphoric acid (85 wt %, 0.01 mL, 0.1 mol%) was added and the solution was heated at 120 °C while distilling off the so-formed water (c.a. 30 min). After that, the product **3a** was distilled off and weighted (111 °C, 1 mmHg, 2.36 g, 17 % yield).

2.4.3. High-scale experimental procedure for 1:1 ketone: alcohol ratio with DTBP radical initiator

CDDK **2** (18.2 g, 100 mmol) was placed in a two-necked 50 mL round-bottomed flask equipped with a magnetic stir bar, a pressure-compensated addition funnel and a condenser fitted with a nitrogen balloon, and then heated in an oil bath at 140 °C. A solution of *tert*-butyl peroxide DTBP (10.8 mL, 30 mol%) in allyl alcohol **1a** (7.3 mL, 100 mmol) was poured into the addition funnel during 30 min. After that time the mixture was left to stir at 140 °C for additional 6 h and then the corresponding acid solid catalyst (2.0 g) or phosphoric acid (85 wt%, 0.05 mL, 0.1 mol%) was added to the solution, heated at 120 °C. After that, the mixture was analyzed by ^{1}H nuclear magnetic resonance (NMR) spectroscopy and also by gas chromatography coupled to mass spectrometry (GC–MS) after diluting in $CDCl_3$, using prepared standards as a calibrate. The calculated **3a** (based on ketone and not in allyl alcohol) yield is 7%.

2.4.4. Reproduction of industrial reaction conditions

CDDK **2** (50.0 g, 274.7 mmol) was placed in a two-necked 100 mL round-bottomed flask equipped with a magnetic stir bar, a pressure-compensated addition funnel and a condenser, and heated in an oil bath at 140 °C. A solution of *tert*-butyl peroxide DTBP (4.4 mL, 30 mol%) in allyl alcohol **1a** (5.5 mL, 75 mmol) was poured into the addition funnel and added dropwise during 6 h. After that time, the mixture was left to stir at 140 °C for additional 3 h and then the excess CDDK **2** was distilled off through a 10 cm long Vigreaux column (107 °C, 13 mmHg, 40.3 g, >99 % recovering). Then, the corresponding acid solid catalyst (5.0 g) or phosphoric acid (85 wt%, 0.05 mL, 0.1 mol%) was added and the solution was heated at 120 °C while distilling off the so-formed water (c.a. 30 min). After that, product **3a** was distilled off in pure form (111 °C, 1 mmHg, 10.8 g, 17 % yield).

3. Results and Discussion

3.1. Catalytic radical α–alkylation of cyclododecanone (CDDK) with biomass–derived reagents

Table 1 shows the coupling reaction between allyl alcohol derivatives **1a–d** and cyclododecanone **2** (CDDK) under open air conditions, at different reaction temperatures. From >20 radical organic and metal catalysts tested, [9] only DTBP (entries 5–8) and Mn^{2+} salts, either in anhydrous or aqueous form (i.e. entries 21–23), gave >10 % yields of the alkylated products **3a–b**. In particular, the $Mn(OAc)_2$ catalyst achieves ca. 40 % yield under 4 atmospheres of O_2 (entries 24–26), and ca. 55 % yield when the biomass–derived reagent allyl hexanoate (**1c**, R^1= *n*–hex) and hexanoic acid solvent were used, either under pure oxygen atmospheres (entry 27) or simulated air (entry 28, see optimization tests in Tables S1–S2 and Figure S1). Other Mn catalysts were also reasonable effective (entries 30–33), but less active than the corresponding acetate salt. The beneficial role of acetates to generate the active radicals under aerobic atmosphere will be commented ahead. Although product yields do not exceed 60 %, these results are extraordinary if one considers the number of synthetic steps and waste generation saved, which is dramatically reflected in the final price of the product (see ahead for the fragrance exaltolide).

Kinetic experiments confirm that the biomass–derived derivatives **1c** and hexanoic acid (solvent) are equally effective that the methyl–substituted partners under reaction conditions (Figures S2 and S3). These biomass–derived reagents are not only more sustainable but also circumvent the use of highly flammable and volatile C_{2-4} reagents, whose flammability limits are below 3% in molecular oxygen, according to literature [10a] and to our own measurements (Figure S4). Longer alkyl organic acids also show a satisfactory reactivity, producing a clear benefit in product yield compared to acetic acid and without any significant erosion on selectivity (Table S3). These results are explained by a better solubility of **2** in the longer alkyl chain solvents, since **2** does not completely dissolve in acetic acid even under heating conditions. Indeed, a high hydrophobic substrate such as 1–dodecene **1d** engages well in the coupling with the biomass–derived solvent, giving the highest yield (58 %, entry 29).

3.2. Radical mechanism of CDDK 2 α–alkylation

The industrial process for the alkylation of CDDK **2** with **1a–b** based on DTBP (radical initiator) has, to our knowledge, only been described in patents but not in academic reports, [4a] and the mechanism is not yet understood. This lack of knowledge about a challenging but applied organic reaction is surprising. Thus, the mechanisms for both the DTBP radical initiator and the Mn^{2+} catalyst will be studied here, taking as a reaction model the alkylation of CDDK **2** with **1a** or **1b**, in order to stablish parallelisms and differences.

3.2.1. Radical mechanism with the DTBP initiator

The coupling between CDDK **2** and **1a** initiated by DTBP proceeds with a first–order kinetics in the initial 1–2 h of reaction, and then rapidly leverages, regardless the amounts of reagent used (Figure S5). The rate equation obtained with different amounts of each reactant (ketone **2**, alkene **1a** and DTBP) and different temperatures, is $r_0=k_{app}$ [2][DTBP] (k_{app}= an apparent rate constant), which suggests that the abstraction of the α hydrogen atom in **2** is the rate–determining step (rds) of the reaction. The fact that thermally sensitive but much more reactive peroxy radicals such as $(^{t}BuCOO)_2$ and $(^{t}BuON)_2$ gave significant amounts of **3a** (entries 9 and 10 in Table 1), supports this hypothesis.

A combined analysis of the liquid and gas phase during reaction by GC and ^{1}H NMR shows that the conversion of **1a** is much faster than the formation of **3a**, that DTBP steadily decomposes to methane, ethane and acetone after 1 h reaction time, and that product **3a** also decomposes under reaction conditions, as assessed with neat **3a** (isolated by column–chromatography, Figures S6 and S7). Control experiments show that the rate of degradation of **3a** is just slightly lower than its formation (~15 % h^{-1}) in the presence of the peroxide, which explains the sudden stopping of the reaction. Indeed, if more DTBP is added when the reaction stops, the yield of **3a** does not increase beyond an additional 1%. Product **3a** does not degrade (<5% after 2 h) without DTBP. These results strongly suggest that **1a** and **3a** decompose during reaction by the aggressiveness of the radicals, thus the formation of **3a** by the DTBP–mediated reaction is intrinsically limited. [10b] This degradation is directly related to the presence of more acid hydrogen atoms in the product than in the reactants (see Figure S8 for pKas), which explains the better results obtained with allyl derivatives **1b–d** respect to allyl alcohol **1a**. The use of reagents that may alleviate radical degradation such as bases, organic molecules (*N*–hydroxyphthalimide, NHPI), radical trapping metals (copper), acetone and hydrophobic solvents do not produce significant improvements (Table S8 and Figures S9–S11). Despite the use of allyl acetate **1b** allows to increase the amount of peroxide without suffering severe decomposition, even after addition in twice (Table S5), and GC and NMR measurements confirm the better stability and isolation (Figure S12) of product **3b** under reaction conditions (Figure S13), degradation still occurs and none of the palliative methods tested with **1a** worked with **1b** (Figure S14).

With the above results in hand, Fig. 2 shows the proposed mechanism for the radical addition of alkenes to CDDK **2** initiated by DTBP, which consists in peroxide homolytic fragmentation, *H* abstraction from **2** and final coupling with the alkene. The *O*–centered radical of DTBP decomposes to a *C*–centered radical and acetone, which consumes the DTBP and significantly degrades reagents and product (Figure S15).

3.2.2. *Radical mechanism with the Mn^{2+}/O_2 catalyst*

The rate equation obtained with different amounts of each reactant (**2**, **1b**, $Mn(OAc)_2{\cdot}4H_2O$, O_2 and acid solvent) for the Mn^{2+}–catalyzed process is $r_0=k_{app}$ [2][Mn][O_2][acid solvent] (k_{app}= an apparent rate constant), thus resembling that of DTBP but changing the organic peroxide by the combination of Mn^{2+} catalyst, air and the organic acid solvent (Figure S16). The use of stoichiometric amounts of Mn $(OAc)_2{\cdot}4H_2O$ under N_2 did not give any conversion of **2**, which indicates that Mn^{2+} does not transfer electrons to **2** unless O_2 is present, and when so, CO_2 extrusion and C—C breaking of **2** are also observed (Figure S17). These results support the formation of peroxy radicals during the Mn^{2+}–catalyzed reaction. [11a,b] Indeed, if the catalytic Mn^{2+}/O_2 system is replaced by peracetic acid, the reaction proceeds with a similar first order kinetics. No other solvents rather than alkyl carboxylic acids are active for the reaction (see Figure S16). These results, together, indicate that peracid species are catalytically formed from Mn^{2+}, O_2 and the solvent during reaction, and that this peracid is the true active radical initiator of the coupling, which nicely explains the equation rate obtained. Although the transformation of Mn^{2+} acetate to Mn oxide during reaction is a possibility, [11c] the fact that MnO is the less active of all Mn catalysts (Table 1, entry 30) and that the reaction is performed in a high excess of AcOH or other carboxylic acid (see also ahead), strongly suggests that the catalytic Mn site is in acetate form. The mechanism proposed for the Mn^{2+}–catalyzed coupling of **2** with **1b** is shown in Fig. 3, above.

3.3. *Mn^{2+}–zeolites as recyclable solid catalysts*

The transformation of homogeneous into heterogeneous catalytic process is of interest not only from an environmental but also from an industrial point of view, since the solid catalysts can be recovered, recycled and ultimately engineered in continuous flow. [12a–c] Radical catalysts dissolved in acetic acid are very difficult to translate into recyclable solids, since the extreme polarity of the reaction medium favors a rapid leaching of the catalytic species. [12d] However, the use of longer alkyl organic acids instead of acetic acid as a solvent enables here the possibility of having metal supported catalysts without leaching. Table 2 shows the results for different Mn^{2+}–supported solid catalysts under the optimized conditions for the homogenous system. Mn $(OAc)_4{\cdot}4H_2O$ is still active when supported by impregnation on silica, however, the catalytic activity corresponds exclusively to Mn^{2+} species leached into the solution, as it may be expected from a low metal–support interaction. This result indicates that the Mn^{2+} catalytic species must be more tightly anchored on the solid surface in order to have a recyclable catalyst, otherwise leaching will occur. Thus, zeolites were envisioned as potential support candidates, since the silico–alumina structure should not interfere in the radical process, as silica does, but the anionic network of the zeolite may further stabilize Mn^{2+} cationic species, avoiding leaching [13]. Besides, zeolites are active matrixes for radical reactions of ketones and aldol–type transformations [13a–f].

The representative zeolites Y and Beta, in Na, NH_4 and H ionic forms, were tested as supports for Mn^{2+}, since these 3D zeolites present a pore opening of ~7 Å, wide enough to diffuse the reagents and products of the reaction (see Figure S18 for zeolite details) [13]. Recalling that other Mn^{2+} species are also catalytically active (see entries 30–33 in Table 1 above), the catalytic Mn^{2+} species were supported here not only by impregnation but also by aqueous cationic exchange of $Mn(OAc)_4{\cdot}4H_2O$ with the zeolite cations, since the latter enables a stronger ionic interaction between the zeolite and Mn^{2+}, at expenses of removing acetate ligands. The loading of Mn^{2+} supported by ionic exchange depends on the zeolite employed and ranges in 1.7–2.2 wt% (Figure S18) according to inductively coupled plasma atomic emission spectroscopy measurements (ICP–AES), after disaggregating the solid in concentrated HF solutions. With this result in hand, the impregnation of the zeolites was carried out with similar amounts of $Mn(OAc)_4{\cdot}4H_2O$ (~1.5 wt%), in order to have comparative results. The comparative characterization of Mn^{2+}–NaBeta with the pristine zeolite by powder X–ray diffraction (XRD, Figure S19), Fourier–transformed infrared spectra (IR, Figure S20) and high–resolution field emission scanning electron microscopy (HR–FESEM, Figure S21) shows that the microstructure remains unaltered after Mn^{2+} incorporation. Besides, Mn is hardly detected in the energy dispersive X–ray spectra of the sample during FESEM measurements, thus indicating a good incorporation and dispersion of Mn within the zeolite framework. X–ray photoelectron microscopy (XPS, Figure S22) shows a binding energy for Mn^{2+} around 645 eV, attributable to [MnO_4], [11c] in other words, the Mn^{2+} sites are surrounding by multiple hydroxyl groups of the zeolite walls, as it may be expected. These results, together, confirm the incorporation of Mn^{2+} in cationic positions within the zeolite.

The catalytic results in Table 2 show that all the zeolites worked well as a catalyst for the coupling of CDDK **2** with allyl acetate **1b**, with general yields of **3b** ca. 20–40 % for both the impregnated and the exchanged zeolites, except for zeolite HBeta. In general, the non–acid zeolites worked better than the acid ones, and remarkably, the exchanged zeolites worked better than the impregnated zeolites, particularly Mn^{2+}–NaBeta, which gave a 48 % yield of **3b**, a better yield than any homogeneous catalyst tested. These results strongly suggest that the zeolite framework can isolate Mn cations by ion exchange, stabilizing Mn^{2+} to efficiently catalyze the radical reaction [14]. Fig. 3 shows the hot filtration test for the reaction with Mn^{2+}–NaBeta as a catalyst, and the catalytic activity coming from species in solution is 14 % of the total (4% out of 28 % after filtration). ICP–AES analyses showed a loss of 0.19 Mn wt% in the solid after use and a 0.14 Mn wt% in the reaction filtrates, which match the percentage of catalytic activity in solution. In addition, Fig. 3 also shows that Mn^{2+}–NaBeta can be recycled three times but with a continuous decrease of catalytic activity throughout the results, due to the systematic loss of Mn, as confirmed by ICP–AES analyses. Nevertheless, although the solid catalyst presents some leaching and the consequent loss of activity throughout the reuses, these results open the way to design solid catalysts for radical–catalyzed aerobic transformations in acidic organic media, and bring a rare

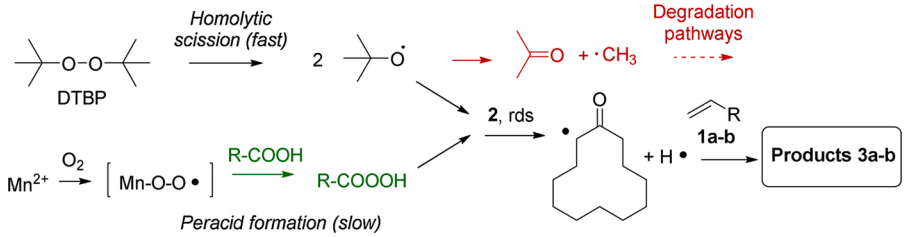

Fig. 2. Proposed reaction mechanisms for the α–alkylation of **2** with the radical initiator DTBP and Mn^{2+}/O_2/alkyl acid catalysts.

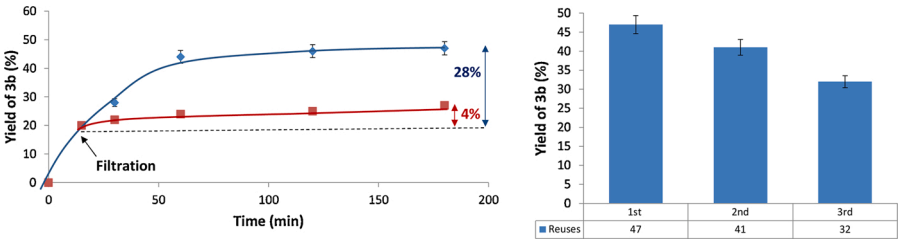

Fig. 3. Hot filtration test (left) and reuses (right) of Mn^{2+}–NaBeta catalyst during the α–alkylation of CDDK **2** with allyl acetate **1b** under optimized reaction conditions (see Table 2). Error bars account for 5% uncertainty.

Table 2
Results for the catalytic radical coupling of allyl acetate 1b with CDDK 2 under aerobic conditions.

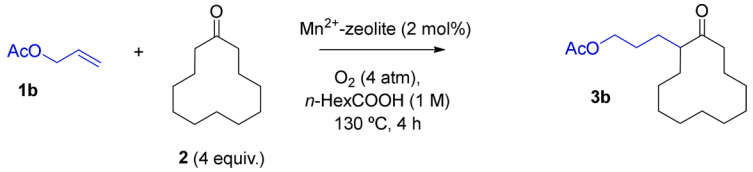

Entry	Catalyst	Synthetic method	3b (%)
1	$Mn(OAc)_2$–SiO_2	Impregnation	30[a]
2	$Mn(OAc)_2$–NaY	Impregnation	29
3	Mn^{2+}–NaY	Ionic exchange	21
4	$Mn(OAc)_2$–HY	Impregnation	21
5	Mn^{2+}–HY	Ionic exchange	38
6	$Mn(OAc)_2$–NaBeta	Impregnation	30
7	**Mn^{2+}–NaBeta**	**Ionic exchange**	**47**
8	$Mn(OAc)_2$–NH_4Beta	Impregnation	27
9	Mn^{2+}–NH_4Beta	Ionic exchange	43
10	$Mn(OAc)_2$–HBeta	Impregnation	<5
11	Mn^{2+}–HBeta	Ionic exchange	17

[a] Complete leaching of Mn observed.

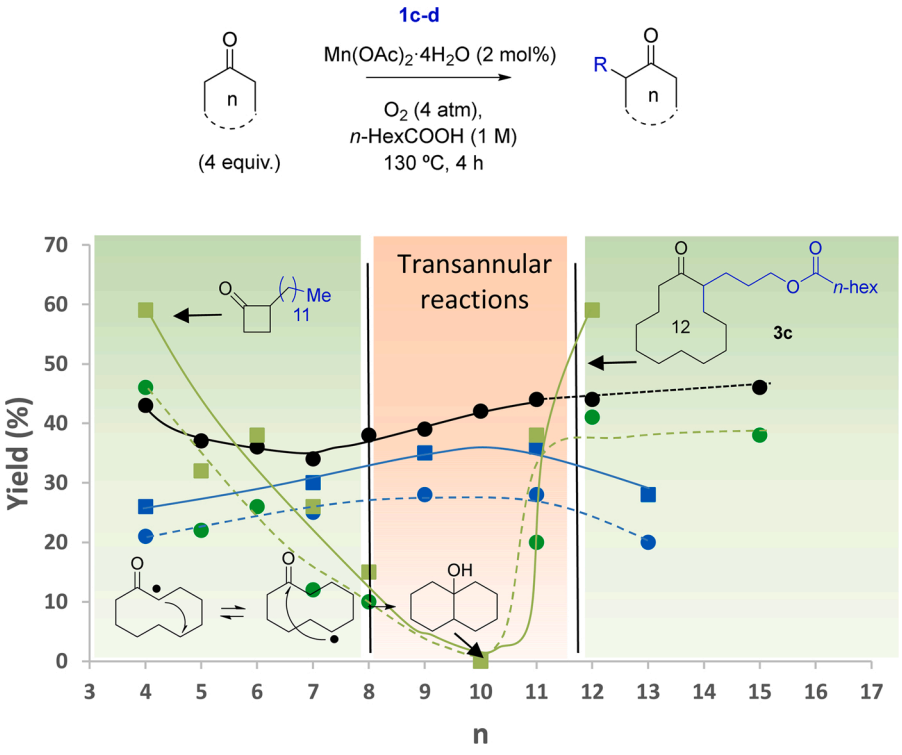

Fig. 4. Yields of the radical α–alkylation of cyclic and acyclic ketones with allyl hexanoate **1c** and 1–dodecene **1d** under the indicated conditions. Black points are the reported electron affinities for cyclic ketones in Kcal·mol^{-1} (aprox. + 2.0 for acyclic ketones), with the last two data extrapolated (dash line).[16] Green points are the experimental yields for cycle ketones (circles for reaction with **1c** and squares for reaction with **1d**) and blue points are the experimental yields for linear ketones (same coding). Lines are a guide to the eye.

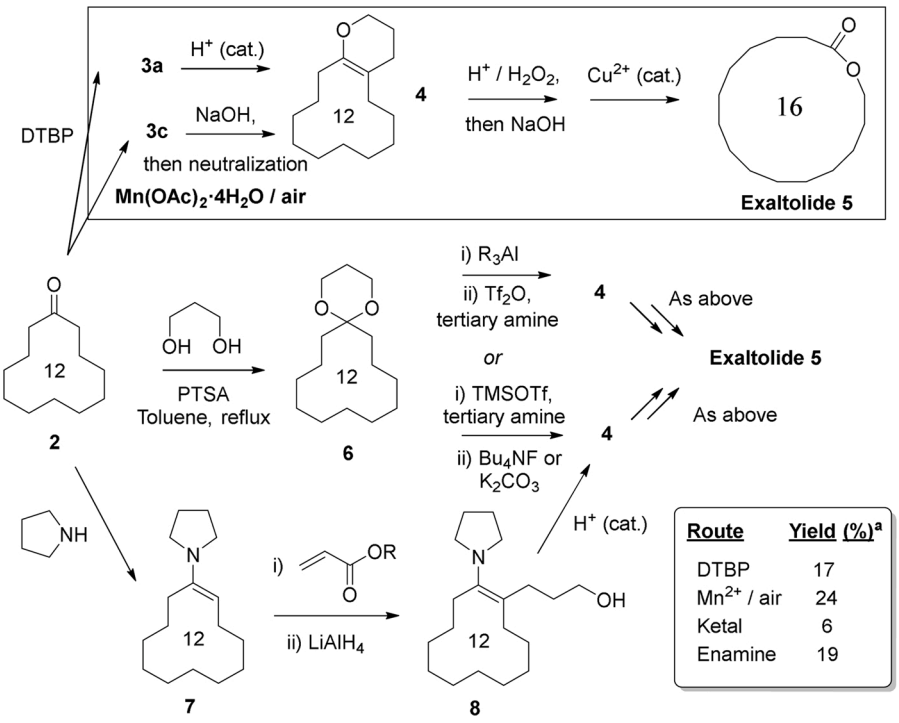

Fig. 5. Synthesis of exaltolide **5** from CDDK **2** by different routes. [a] Overall isolated yield at >0.5 g–scale.

example of solid–catalyzed α–alkylation of zeolites with simple alkenes [15]. Characterization of the used zeolite shows that the microstructure is preserved (see Figures S19-S20).

3.4. *The uniqueness of large cyclic and alkyl ketones for the radical α–alkylation*

Molecular polarization is a well–known effect in ketones, clearly reflected not only into the physicochemical properties (boiling point, refractive, index,…) but also in the spectroscopic values (carbonyl NMR and IR shifts,…) which, however, has barely been correlated with reactivity [5]. Fig. 4 shows the yield obtained for the radical coupling of different cyclic and acyclic ketones with both allyl hexanoate **1c** and 1–dodecene **1d**, under the optimized conditions in Table 1 (2 mol% of $Mn(OAc)_4{\cdot}4H_2O$, 130 °C) *vs.* the number of carbon atoms (*n*) in the cycle/chain. It can be seen that, regardless the type of ketone and alkene employed, yields of alkylated ketone parallel their electronic affinity, which is an accepted parameter to measure the molecular polarization [16].

The higher radical α−alkylation observed for ketones of increasing length means that the reaction depends linearly on the ability of the alkyl moiety to stabilize the radical by inductive effects, except for medium–size cycles up to cyclodecanone ($\leq C_{10}$), where full conversion is observed but without any alkylation product [17]. GC and NMR analyses of the reaction mixture of cyclodecanone (C_{10}) show the formation of no less than 10 new products, from which >70 % corresponds to decaline products, together with some dimerization and minor unidentified products. As depicted in Fig. 4, the decaline mixture is produced by rapid radical rearrangement and transannular reactions, [6] which explains the lack of α–alkylation for medium–size cycles. Thus, it can be said that the radical α–alkylation of ketones can be predicted on the basis of the ketone structure, which is a sound starting point for the design of new reactions.

3.5. *Synthesis of exaltolide*

Exaltolide **5** is a widely–used marketed fragrance molecule, currently manufactured at multi–ton amounts from **3a** with DTBP as a sub–stoichiometric reagent. Fig. 5 shows the overall isolated yields obtained for exaltolide **5**, in our hands, for a) the current industrial DTBP process,[4a] b) the aerobically Mn^{2+}–catalyzed procedure, and c) other alternative processes reported in the literature (see details for each procedure in Figures S23–27) [7a,18,19]. All the routes have in common the synthesis of intermediate α–alkylated cyclododecanones **3** and cyclopyrane **4**, which is in turn converted to exaltolide **5** [20].

The highest yield of exaltolide **5** (24 %) is obtained by the Mn^{2+}/air route described here which, besides, is the shortest route (4 steps, Figure S23). The current industrial route [4a] gives a lower yield (17 %, Figure S24) than the Mn^{2+}/air route and uses the low sustainable and more expensive organic peroxide in sub–stoichiometric amounts, which translates in a calculated economic increase of ≈1 million euros for an annual production of 500 tons [21]. The ketal route [19] makes use of the intermediate ketal **6** to achieve exaltolide **5** after several steps with expensive reagents (Figures S25–26) and to give the lowest yield of the synthetic pathways tested (6%). The enamine route [18] has not been reported before, as far as we know, for the synthesis of **5**, but just for intermediates **7** and **8**. We have here completed the synthesis of **5** to give, in our hands, a respectable yield (19 %, Figure S27), however, the complete route requires 7 steps with expensive reagents. These results showcase the effectiveness of the Mn^{2+}–catalyzed aerobic process, beyond the intrinsic environmental and practical advantages associated to biomass–derived reagents and potential solid catalysts.

4. Conclusions

The radical α–alkylation of ketones with unactivated alkenes proceeds with earth–abundant, cheap and non–toxic Mn^{2+} catalysts by a biomass–based industrial aerobic process, to enable the multi–ton industrial fragrance exaltolide **5** in significantly higher yields than any other reported method, including the current industrial route. A combination of high polarizability, high steric hindrance for dimerization and lack of proximity effects, makes large cyclic ketones particularly suitable to engage in this full–atom economic radical α–alkylation reaction. A simple solid catalyst based on Mn^{2+}–supported zeolites bring

promising results for the design of a process based on heterogeneous catalysts. The consideration of perhaps old but sound organic concepts to explain cyclic ketone reactivity poses a new scenario for the application of ketones in industrial processes.

Declaration of Competing Interest

The authors have no competing interests to declare.

CRediT authorship contribution statement

Sergio Sanz-Navarro: Investigation, Methodology. **Francisco Garnes-Portolés:** Investigation, Methodology. **Carlos López-Cruz:** Supervision, Validation. **Estela Espinós-Ferri:** Supervision, Project administration, Funding acquisition. **Avelino Corma:** Supervision, Validation, Funding acquisition. **Antonio Leyva-Pérez:** Supervision, Project administration, Writing - original draft, Writing - review & editing.

Acknowledgments

ITQ thanks IFF for its continuous support and collaboration. This work was also supported by the MINECO (Spain) (Projects CTQ2017–86735–P and Excellence Unit "Severo Ochoa" SEV–2016–0683). S. S.–N. thanks MINECO the concession of a FPI contract associated to the above CTQ project, and F. G.–P. thanks ITQ for the concession of a contract.

Appendix A. Supplementary data

Supplementary material related to this article can be found, in the online version, at doi:https://doi.org/10.1016/j.apcata.2021.118021.

References

[1] (a) F. Huang, Z. Liu, Z. Yu, Angew. Chem., Int. Ed 55 (2016) 862–875;
(b) B. Maji, M.K. Barman, Synthesis 49 (2017) 3377–3393;
(c) P. Piehl, R. Amuso, E. Alberico, H. Junge, B. Gabriele, H. Neumann, M. Beller, Chem. Eur. J. 26 (2020) 6050–6055.

[2] (a) M. Nakamura, T. Hatakeyama, E. Nakamura, J. Am. Chem. Soc. 126 (2004) 11820–11825;
(b) F. Mo, G. Dong, Science 345 (2014) 68–72;
(c) Y. Dang, S. Qu, Y. Tao, X. Deng, Z.-X. Wang, J. Am. Chem. Soc. 137 (2015) 6279–6291;
(d) Z. Huang, H.N. Lim, F. Mo, M.C. Young, G. Dong, Chem. Soc. Rev. 44 (2015) 7764–7786;
(e) D. Xing, G. Dong, J. Am. Chem. Soc. 139 (2017) 13664–13667;
(f) X. Li, H. Wu, Y. Lang, G. Huang, Catal. Sci. Technol. 8 (2018) 2417–2426;
(g) D. Xing, X. Qi, D. Marchant, P. Liu, G. Dong, Angew. Chem., Int. Ed 58 (2019) 4366–4370;
(h) H.N. Lim, D. Xing, G. Dong, Synlett 30 (2019) 674–684.

[3] (a) A. Mastracchio, A.A. Warkentin, A.M. Walji, D.W.C. MacMillan, Proc. Natl. Acad. Sci. 107 (2010) 20648–20651;
(b) F. Lima, U.K. Sharma, L. Grunenberg, D. Saha, S. Johannsen, J. Sedelmeier, E. V. Van der Eycken, S.V. Ley Angew, Chem., Int. Ed 56 (2017) 15136–15140.

[4] (b) T. Iwahama, S. Sakaguchi, Y. Ishii, Chem. Commun. (2000) 2317–2318;
R. Hopp, K. Bauer, USA patent 3856815, (1974).

[5] (a) J. Applequist, J.R. Carl, K.-K. Fung, J. Am. Chem. Soc. 94 (1972) 2952–2960;
(b) I.A. Blair, J.H. Bowie, V.C.J. Trenerry, Chem. Soc., Chem. Commun. (1979) 230–231;
(c) K.A. Bode, J. Applequist, J. Phys. Chem. 100 (1996) 17820–17824;
(d) D.A. Walthall, J.M. Karty, B. Römer, O. Ursini, J.I. Brauman, J. Phys. Chem. A 109 (2005) 8785–8793.

[6] (a) M. Szostak, L. Yao, J. Aubé, J. Am. Chem. Soc. 132 (2010) 2078–2084;
(b) E. Reyes, U. Uria, L. Carrillo, J.L. Vicario, Tetrahedron 70 (2014) 9461–9484.

[7] (a) N. Hanaki, K. Ishihara, M. Kaino, Y. Naruse, H. Yamamoto, Tetrahedron 52 (1996) 7297–7320;
S. Lambrecht, W. Marks, H.-J. Topp, N. Richter, W. Kuhn, US 2005/0085536 A1 (2005). (d) X. Shen, T.T. Nguyen, M.J. Koh, D. Xu, A.W.H. Speed, R.R. Schrock, A. H. Hoveyda, Nature 541 (2017) 380–386.

[8] (a) W. Hui, C. Isaac, R. Torben, K. Nikolaos, A. Lutz, Nat. Catal. 1 (2018) 993–1001. For Mn–catalyzed alkene reactions see:;
(b) V. Papa, Y. Cao, A. Spannenberg, K. Junge, M. Beller, Nat. Catal. 3 (2020) 135–142;
(c) T. Liu, Y. Yang, C. Wang, Angew. Chem., Int. Ed 59 (2020) 14256–14260;
(d) M. Pena–Lopez, P. Piehl, S. Elangovan, H. Neumann, M. Beller, Angew. Chem., Int. Ed 55 (2016) 14967–14971. For Mn–catalyzed ketone alkylation reactions see:;
(e) M. Milan, M. Bietti, M. Costas, ACS Cent. Sci. 3 (2017) 196–204. For Mn–catalyzed peroxide–mediated reactions see:;
(f) A. Corma, S. Iborra, A. Velty, Chem. Rev. 107 (2007) 2411–2502. For a representative review on biomass see:;
(g) U. Linker, B. Kersten, T. Linker, Tetrahedron 51 (1995) 9917–9926. For catalytic Mn^{3+} see:.

[9] A. Kockritz, R. Eckelt, O. Koch, P. Esser, J. Panten, W. Baumann, H. Atia, Eur. J. Inorg. Chem. 2018 (2018) 2776–2784.

[10] (a) P.M. Osterberg, J.K. Niemeier, C.J. Welch, J.M. Hawkins, J.R. Martinelli, T. E. Johnson, T.W. Root, S.S. Stahl, Org. Process Res. Dev. 19 (2015) 1537–1543;
(b) M. Martin–Martinez, R.S. Ribeiro, B.F. Machado, P. Serp, S. Morales–Torres, A. M.T. Silva, J.L. Figueiredo, J.L. Faria, H.T. Gomes, ChemCatChem 8 (2016) 2068–2078.

[11] (a) X. Zhao, T. Zhang, Y. Zhou, D. Liu, J. Mol. Catal. A Chem. 271 (2007) 246–252;
(b) G. Luo, X. Lu, X. Wang, S. Yan, X. Gao, J. Xu, H. Ma, Y. Jiao, F. Li, J. Chen RSC Adv. 5 (2015) 94164–94170;
(c) E. Karakhanov, A. Maximov, A. Zolotukhina, V. Vinokurov, E. Ivanov, A. Glotov, Catalysts 10 (2020) 7.

[12] (a) L. Liu, A. Corma, Chem. Rev. 118 (2018) 4981–5079. For recent reviews see;
(b) J.R. Cabrero–Antonino, R. Adam, V. Papa, M. Beller, Nat. Commun. 361 (2019) 185–191;
c) M. Viciano–Chumillas, M. Mon, J. Ferrando–Soria, A. Corma, A. Leyva–Pérez, D. Armentano, E. Pardo, Acc. Chem. Res. 53 (2020) 520–531;
(d) P. Kalck, C. Le Berre, P. Serp, Chem. Rev. 402 (2020), 213078. For reactions in acetic acid see.

[13] (a) H.Y. Luo, L. Bui, W.R. Gunther, E. Min, Y. Roman–Leshkov, ACS Catal. 2 (2012) 2695–2699;
(b) P. Wu, Y. Kubota, T. Yokoi, ACS Catal. 4 (2014) 23–30;
(c) S. Van de Vyver, Y. Roman–Leshkov, Angew. Chem., Int. Ed 54 (2015) 12554–12561;
(d) T. Ennaert, J. Van Aelst, J. Dijkmans, R. De Clercq, W. Schutyser, M. Dusselier, D. Verboekend, B.F. Sels, Chem. Soc. Rev. 45 (2016) 584–611;
(e) Y. Wang, J.D. Lewis, Y. Roman–Leshkov, ACS Catal. 6 (2016) 2739–2744;
(f) J.D. Lewis, M. Ha, H. Luo, A. Faucher, V.K. Michaelis, Y. Roman–Leshkov, ACS Catal. 8 (2018) 3076–3086;
(g) A. Rodriguez–Fernandez, J. Di Iorio, C. Paris, M. Boronat, A. Corma, Y. Roman–Leshkov, M. Moliner, Chem. Sci. 11 (2020) 10225–10235;
(h) M.A. Rivero–Crespo, J. Oliver–Meseguer, K. Kapłońska, P. Kuśtrowski, E. Pardo, J.P. Cerón–Carrasco, A. Leyva–Perez, Chem. Sci. 11 (2020) 8113–8124;
(i) M.A. Rivero–Crespo, M. Tejeda–Serrano, H. Pérez–Sánchez, J. P. Cerón–Carrasco, A. Leyva–Pérez, Angew. Chem. Int. Ed 59 (2020) 3846–3849;
(j) M. Mon, R. Bruno, S. Sanz–Navarro, C. Negro, J. Ferrando–Soria, L. Bartella, L. Di Donna, M. Prejanò, T. Marino, A. Leyva–Pérez, D. Armentano, E. Pardo, Nat. Commun. (2020) 3080, https://doi.org/10.1038/s41467–020–16699–3. For other related micro–structured materials, such as MOFs, see:.

[14] (a) P. Rubio–Marqués, M.A. Rivero–Crespo, A. Leyva–Pérez, A. Corma, J. Am. Chem. Soc. 137 (2015) 11832–11837;
(b) I.C. Gerber, P. Serp, Chem. Rev. 120 (2020) 1250–1349;
(c) M. Tejeda-Serrano, S. Sanz–Navarro, F. Blake, A. Leyva-Pérez Synthesis 52 (2020) 2031–2037.

[15] G. Meng, M. Patel, F. Luo, Q. Li, C. Flach, R. Mendelsohn, E. Garfunkel, H. He, M. Szostak, Chem. Comm. 55 (2019) 5379–5382.

[16] (b) A.H. Zimmerman, R.L. Jackson, B.K. Janousek, J. Brauman, J. Am. Chem. Soc. 100 (1978) 4674–4676.

[17] J.S. Sharley, A.M. Collado–Pérez, E. Espinos–Ferri, A. Fernandez–Miranda, I. R. Baxendale, Tetrahedron 72 (2016) 2947–2954.

[18] J.R. Mahajan, H. de Araujo, Synthesis 1980 (1980) 64–66.

[19] P.G. Gassman, S.J. Burns, K.B. Pfisterl, J. Org. Chem. 58 (1993) 1449–1457.

[20] Y.N. Ogibin, A.O. Terentév, G.L. Nikishin, Russ. Chem. Bull. 47 (1998) 1166–1169.

[21] Corma A., Leyva–Pérez, A., Espinós–Ferri, E., López–Cruz, C., European patent number 16382632.4–1451 (2016) and USA patent 15833455 (2017).